ACS OMEGA

http://pubs.acs.org/journal/acsodf

Article

Novel Span-PEG Multifunctional Ultrasound Contrast Agent Based on CNTs as a Magnetic Targeting Factor and a Drug Carrier

Jie Zhang, Zhongtao Liu, Shujing Zhou, Yang Teng, Xiangyu Zhang, and Jinjing Li*

Cite This: *ACS Omega* 2020, 5, 31525−31534

Read Online

ACCESS | Metrics & More | Article Recommendations

ABSTRACT: Based on the targeting of ferroferric oxide (Fe_3O_4) and the drug-loading property of carbon nanotubes (CNTs), a novel Span-PEG-composited Fe_3O_4−CNTs−DOX multifunctional ultrasound contrast agent was designed and applied to tumor lesions. In situ liquid phase synthesis was employed to prepare the Fe_3O_4−CNTs magnetic targeting complex, and the physical method was used to obtain the Fe_3O_4−CNTs−DOX complex by loading doxorubicin (DOX) onto Fe_3O_4−CNTs. The targeted drug-loading complex Fe_3O_4−CNTs−DOX was combined with the membrane material of Span-PEG by the acoustic vibration cavitation method. The maximum tolerance for Span-PEG-composited Fe_3O_4−CNTs−DOX microbubbles was 450 times higher, which has good safety. The loading rate of DOX in the obtained composite microbubbles was 17.02%. The proliferation inhibition rate of Span-PEG-composited Fe_3O_4−CNTs−DOX microbubbles on liver cancer SMMC-7721 cells reached 48.3%. Span-PEG-composited Fe_3O_4−CNTs−DOX microbubbles could significantly enhance ultrasonic imaging and enrich at a specific location under an external magnetic field, and the extended imaging time could ensure the effective observation and diagnosis of lesions.

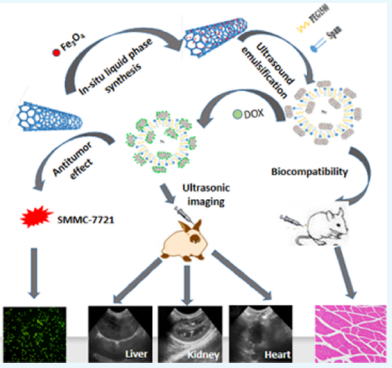

1. INTRODUCTION

A targeted microbubble ultrasound contrast agent is a contrast agent that can carry targeting factors and target imaging, can also deliver drugs or genes, and has a therapeutic effect. Specific imaging of target tissue can be achieved at the early stage of disease by its specific binding to target cell surface markers. Nowadays, the applications of the targeted microbubble ultrasound contrast agent in tumor targeting, imaging, and treatment are hot spots for researchers. Lu et al.[1] synthesized the nanobubbles (NBs) that were modified by ferrous protoporphyrin (FH) and loaded with doxorubicin, FH-NB-DOX; multifunctional nanobubbles of 208 nm showed good ultrasound contrast and could deliver more DOX to cancer-associated fibroblasts (CAFs) and inhibit tumor growth under ultrasound irradiation, which had a stronger eradication effect than free DOX.

At present, although paclitaxel and doxorubicin as the main drugs for cancer treatment have a good tumor suppression effect, yet they can cause systemic toxicity due to the lack of tumor targeting. A nano drug-loading system can achieve drug-targeted delivery and includes liposomes, polymer micelles, polymer nanoparticles, nanogels, and carbon nanotubes (CNTs).[2−4] As one of the most advanced nanocarriers for efficiently delivering drugs and biomolecules, CNTs can be noncovalently or covalently combined with different drugs, biomolecules, and nanoparticles.[5−7] Yan et al.[8] developed a novel actively targeting and pH-responsive system for delivering the drug doxorubicin (DOX) to tumor sites using folic acid (FA)-modified multiwalled carbon nanotubes (MWCNTs). The FA-bound MWCNTs exhibited a high drug loading and an encapsulation efficiency as high as 70.4%. Singh et al.[9] prepared a transferrin-coupled MWCNT nanosystem loaded with docetaxel (DTX); its drug encapsulation rate was as high as 75% and the drug release was ideal. At the same time, CNTs are also an emerging diagnostic imaging tool. The application of CNTs in the ultrasound imaging can enhance ultrasound imaging, increase the drug loading, improve stability, and reduce the sudden release of drugs.[10−13] Deloqu et al.[14] found that CNT could permanently enhance ultrasound contrast, and the ultrasonic signal of functionalized MWCNTs was stronger than that of graphene oxide. Gu et al.[15] used poly(ethylene glycol) (PEG) and anti-prostate-specific membrane antigen (PSMA) aptamers to modify multiwalled carbon nanotubes (MWCNTs) and developed a new type of nanocontrast agent. The results showed that the improved MWCNTs had better visual effects and accuracy and could more effectively target prostate cancer (PCa) cells in comparison with the traditional contrast agents. Fe_3O_4 magnetic nanoparticles have the characteristics of stability, controllability, and strong targeting due to their

Received: July 11, 2020
Accepted: October 12, 2020
Published: December 1, 2020

https://dx.doi.org/10.1021/acsomega.0c03325
ACS Omega 2020, 5, 31525−31534

unique magnetic properties, which make them have broad application prospects in the field of biomedicine. Lv et al.[16] prepared a superparamagnetic Fe_3O_4-ethylenediamine compound that had higher efficacy than free ethylenediamine in inhibiting tumor growth, and the composite nanoparticles could achieve the effect of targeted drug delivery in the presence of an external magnetic field.

This study effectively combined the excellent drug-carrying and imaging functions of CNTs with the superparamagnetism of Fe_3O_4 nanoparticles and applied them in an ultrasound contrast agent. A novel type of Span-PEG-composited Fe_3O_4−CNTs−DOX microbubble with multiple effects of ultrasound contrast, targeting, and adjuvant treatment was obtained.

2. RESULTS AND DISCUSSION

XRD of the obtained Fe_3O_4−CNTs complex is shown in Figure 1a. Crystal diffraction peaks at 30.1, 35.6, 43.3, 53.9, 57.3, and 62.8° could be ascribed to six diffraction planes (220), (311), (400), (422), (511), and (440) for Fe_3O_4.[17] A diffraction peak at 26.3° was ascribed to the (002) plane of hexagonal graphite,[18] and the Fe_3O_4−CNTs complex showed the lower strength than the pure CNTs (Figure 1c); this was because the Fe_3O_4 particles on the surface of the CNTs weakened the diffraction peak intensity of CNTs. As a result, the Fe_3O_4−CNTs magnetic targeting complex was successfully synthesized and no crystal impurities were detected.

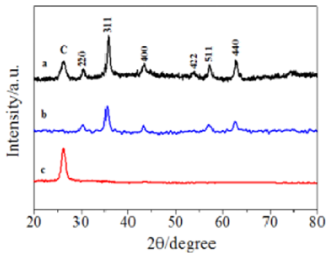

Figure 1. XRD of the Fe_3O_4−CNTs complex (a), Fe_3O_4 (b), and CNTs (c).

SEM of the Fe_3O_4−CNTs complex prepared by in situ liquid phase synthesis is shown in Figure 2. From Figure 2, it can be observed that Fe_3O_4 particles uniformly grew on the surface of CNTs, and the Fe_3O_4−CNTs complex had good magnetism at this time.

Figure 3 shows the hysteresis curve of Span-PEG-composited Fe_3O_4−CNTs microbubbles at room temperature. There was no coercive magnetic field and remanence at the zero point in Figure 3, indicating that the prepared Span-PEG-composited Fe_3O_4−CNTs microbubbles had good magnetic properties.

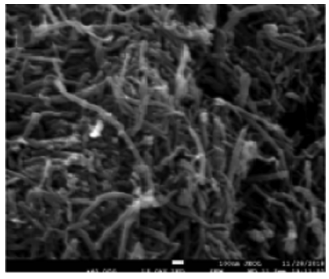

Figure 2. SEM of the Fe_3O_4−CNTs magnetic targeting complex.

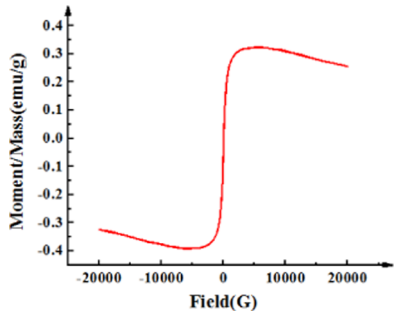

Figure 3. Hysteresis curve of the Span-PEG-composited Fe_3O_4−CNTs microbubble at room temperature.

SEM, TEM, and structure simulation diagram of Span-PEG-composited Fe_3O_4−CNTs microbubbles are shown in Figure 4. Figure 4a shows that the prepared composite microbubbles had a smooth surface and a uniform particle size. It can be seen from Figure 4b that the Span-PEG-composited Fe_3O_4−CNTs microbubble had a hollow structure and its size was nanoscale, and the outer membrane layer of the composite microbubbles showed a black shaded area; its structure simulation diagram is shown in Figure 4c. As described in the previous study,[19,20] Span and PEG as the surfactant molecules formed stable microbubbles that wrapped N_2 inside under the acoustic cavitation. In addition, due to the hydrophilicity of the carboxylated CNTs in the Fe_3O_4−CNTs complex, a part of the Fe_3O_4−CNTs complex would combine to the outer wall of the composite microbubbles. Meanwhile, a small amount of the Fe_3O_4−CNTs complex could also be encapsulated inside the composite microbubble under acoustic vibration.

Figure 5 shows the particle size distribution of Span-PEG-composited Fe_3O_4−CNTs microbubbles. It can be seen from Figure 5 that the size of the composite microbubble was uniform, the average particle size was 425 nm, and the particle size distribution manifested the unimodal form.

After mice were intraperitoneally injected with Span-PEG-composited Fe_3O_4−CNTs microbubbles, there was no acute toxicity such as death in the low-dose group (2000 mg·kg^{-1}) and the middle-dose group (4000 mg·kg^{-1}). In the high-dose group (8000 mg·kg^{-1}), acute toxicity phenomena such as shortness of breath, inattention to diet, and convulsion occurred, and all mice finally died. When the dose exceeded 4500 mg·kg^{-1}, the mice showed acute toxicity phenomena such as shortness of breath and decrease of activity. When the dose reached 6000 mg·kg^{-1}, the mice developed acute toxicity phenomena such as shortness of breath and difficulty of moving, and all finally died. Therefore, Dn = 4500 mg·kg^{-1} and Dm = 6000 mg·kg^{-1} were obtained. As a result, 4500 mg·kg^{-1} was taken as the maximum tolerated dose of mice, and the results of the safety limit experiment are shown in Table 1.

As can be seen from Table 1, when the dose was 4500 mg·kg^{-1}, there was no acute toxicity in mice, so this dose was a safe dose for Span-PEG-composited Fe_3O_4−CNTs microbubbles. Typically, 0.01 g·kg^{-1} was selected as the daily dose of ultrasonic contrast agent for an adult according to the previous study.[19] After calculation, the maximum tolerance multiple of mice was 450 times higher, which was much higher than that of the adult by more than 100 times. It can be seen that the prepared Span-PEG-composited Fe_3O_4−CNTs microbubbles had a high safety.

For the allergic experiment, mice were intraperitoneally injected with Span-PEG-composited Fe_3O_4−CNTs micro-

https://dx.doi.org/10.1021/acsomega.0c03325
ACS Omega 2020, 5, 31525−31534

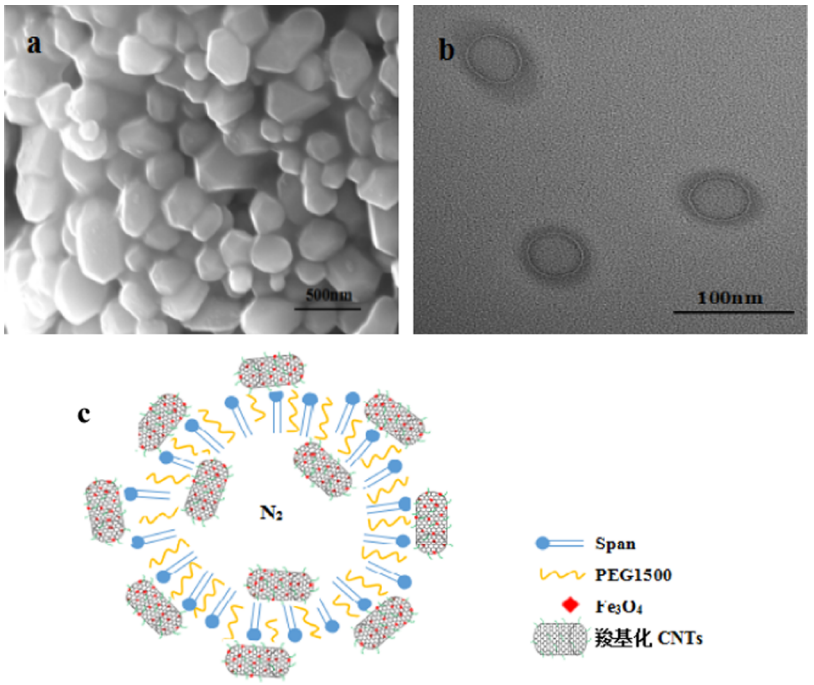

Figure 4. SEM (a), TEM (b), and structure simulation diagram (c) of Span-PEG-composited Fe_3O_4−CNTs microbubbles.[19,20]

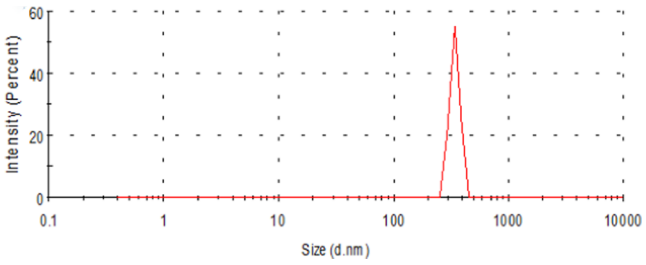

Figure 5. Size distribution of the Span-PEG-composited Fe_3O_4−CNTs microbubble.

Table 1. Acute Toxicity of Span-PEG-Composited Fe_3O_4−CNTs Microbubble on Mice

no.	mice type	gender	dose ($mg \cdot kg^{-1}$)	observation time (days)	acute toxicity
1	KM	male	4500	14	no
2	KM	male	4500	14	no
3	KM	male	4500	14	no
4	KM	male	4500	14	no
5	KM	male	4500	14	no
6	KM	male	4500	14	no
7	KM	male	4500	14	no
8	KM	male	4500	14	no
9	KM	male	4500	14	no
10	KM	male	4500	14	no
11	KM	male	4500	14	no
12	KM	male	4500	14	no
13	KM	male	4500	14	no
14	KM	male	4500	14	no
15	KM	male	4500	14	no
16	KM	male	4500	14	no
17	KM	male	4500	14	no
18	KM	male	4500	14	no
19	KM	male	4500	14	no
20	KM	male	4500	14	no

bubbles at 14 and 21 days after the first muscular administration. Both the groups of mice after injection did not appear to scratch their nose with claws and did not show sneezing, piloerection, convulsions, difficulty in breathing, urine fecal incontinence, shock, and death reaction; as a result, the allergic reaction was judged negative. Moreover, during the first and last administration, the mice in the two groups had a normal diet, water intake, normal weight, glossy coat, and a good mental state. The above experimental results showed that Span-PEG-composited Fe_3O_4−CNTs microbubbles did not cause allergic reactions and sensitization in mice.

In the biocompatibility experiment, mice in the control group were injected with normal saline, and the injection site was observed to be without edema and congestion. Mice in the dose group were injected with Span-PEG-composited Fe_3O_4−CNTs microbubbles, and the injection site was observed to be slightly red by the naked eye at 2 days, the redness disappeared, and there was no obvious abnormality at 4, 10, 22, and 30 days. The stimulation reaction was evaluated according to the following criteria: Grade 0, no obvious reaction; Grade 1, slight hyperemia; Grade 2: moderate hyperemia; Grade 3: severe hyperemia, redness, and swelling, and muscle degeneration; Grade 4, browning, necrosis, and degeneration of muscle; and Grade 5, severe muscle degeneration with mass necrosis. The muscle tissue sections of the injection sites for the saline group and the dose group are shown in Figure 6. Figure 6a shows the muscle tissue sections of mice after injection of normal saline, myofibrils and muscle fibers were neatly arranged under the microscope, and the nucleus was oval and located under the myofilm, indicating no degeneration or necrosis, normal muscle tissue, and reaction level 0. Figure 6b shows the muscle tissue sections at 2 days after the injection of Span-PEG-composited Fe_3O_4−CNTs microbubbles in mice. Inflammatory cell infiltration with the monocytes as a priority and a little cellulose exudation were observed in the local muscle fibers of the muscle tissues, and the reaction was Grade 1. A section of the muscle tissue at

https://dx.doi.org/10.1021/acsomega.0c03325
ACS Omega 2020, 5, 31525−31534

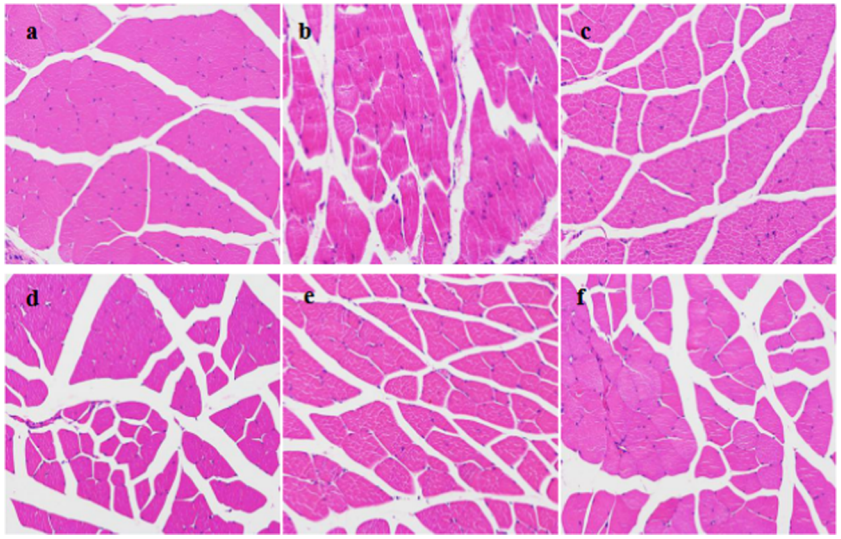

Figure 6. Muscle tissue sections of injection sites of mice: (a) control group and dose groups of (b) 2 days, (c) 4 days, (d) 10 days, (e) 22 days, and (f) 30 days.

4 days after injection (Figure 6c) showed normal muscle tissue and noninflammatory degeneration of the muscle tissue. The muscle tissue sections at 10, 22, and 30 days after injection showed no abnormal lesion in the muscle tissue at the site of administration. The above experimental results showed that injection of Span-PEG-composited Fe_3O_4−CNTs microbubbles had no stimulation, so Span-PEG-composited Fe_3O_4−CNTs microbubbles as an ultrasound contrast agent were biocompatible.

When Span-PEG-composited Fe_3O_4−CNTs−DOX microbubbles were applied to liver cancer SMMC-7721 cells for 12, 24, and 48 h, the inhibitory effect of the composite microbubbles on the proliferation of liver cancer SMMC-7721 cells changed with the microbubble concentration, as shown in Figure 7.

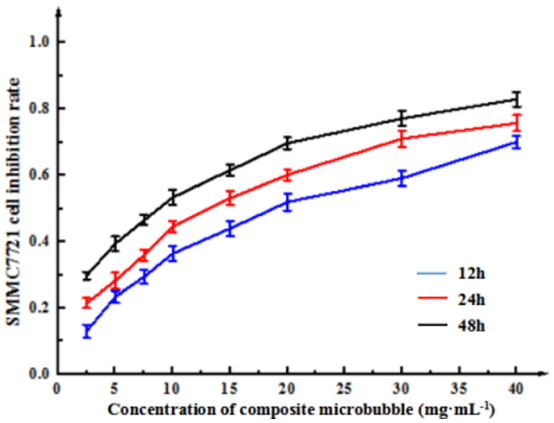

Figure 7. Inhibitory effect of Span-PEG-composited Fe_3O_4−CNTs−DOX microbubbles on Hepatoma SMMC-7721 cells.

It can be seen from Figure 7 that Span-PEG-composited Fe_3O_4−CNTs−DOX microbubbles could inhibit the growth of liver cancer SMMC-7721 cells, and the inhibitory effect of the composite microbubbles on the growth of SMMC-7721 cells was enhanced at different certain with the extension of the action time and the increase of the microbubble concentration. That is, the inhibitory effect showed the following pattern: 48 h > 24 h > 12 h, and the higher the concentration, the better the inhibitory effect, indicating that the inhibition of Span-PEG-composited Fe_3O_4−CNTs−DOX microbubbles on SMMC-7721 cells had dose and time dependence. Moreover, the IC50 values of SMMC-7721 cells were reached in the order of 48, 24, and 12 h. The IC50 for 48 h was small and prone to errors, its incubation time was too long, and it was also easily affected by cell metabolism. The IC50 value of 12 h was too large, and the drug failed to fully interact with cancer cells, resulting in unstable experimental results. Considering the time saving, cost saving, and cell incubation effect, 24 h was selected as the incubation time. SPSS22.0 statistical software analysis showed that the IC50 value for 24 h was 10.36 mg·mL^{-1}.

Figure 8 shows the cytotoxic effects of different microbubbles on liver cancer SMMC-7721 cells and normal mouse

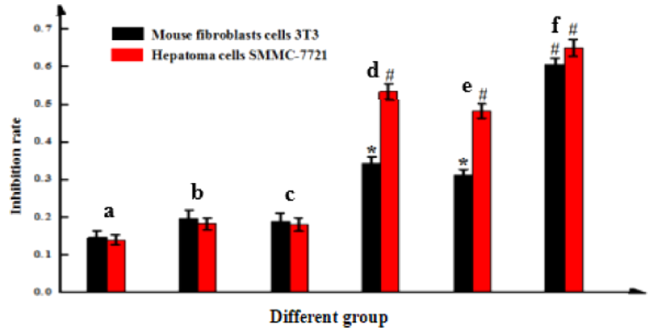

Figure 8. Cytotoxic effects of (a) Span-PEG microbubbles, (b) Span-PEG-composited CNT microbubbles, (c) Span-PEG-composited Fe_3O_4−CNTs microbubbles, (d) Span-PEG-composited CNTs−DOX microbubbles, (e) Span-PEG-composited Fe_3O_4−CNTs−DOX microbubbles, and (f) free DOX.

fibroblast 3T3 cells. After free drug DOX, Span-PEG microbubbles, Span-PEG-composited Fe_3O_4−CNTs−DOX microbubbles, Span-PEG-composited CNTs−DOX microbubbles, Span-PEG-composited Fe_3O_4−CNTs microbubbles, and Span-PEG-composited CNT microbubbles, respectively, were acted on liver cancer SMMC-7721 cells and mouse

https://dx.doi.org/10.1021/acsomega.0c03325
ACS Omega 2020, 5, 31525−31534

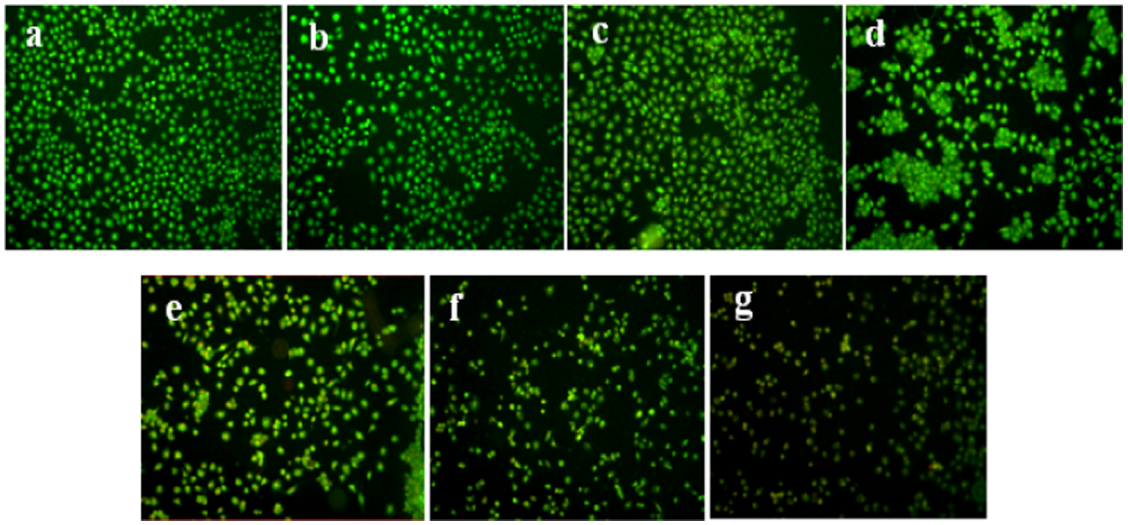

Figure 9. AO/EB staining of hepatoma SMMC-7721 cells: (a) no treatment control group, (b) Span-PEG microbubble group, (c) Span-PEG-composited CNT microbubbles, (d) Span-PEG-composited Fe_3O_4−CNT microbubbles, (e) Span-PEG-composited CNTs−DOX microbubbles, (f) Span-PEG-composited Fe_3O_4−CNTs−DOX microbubbles, and (g) free DOX group.

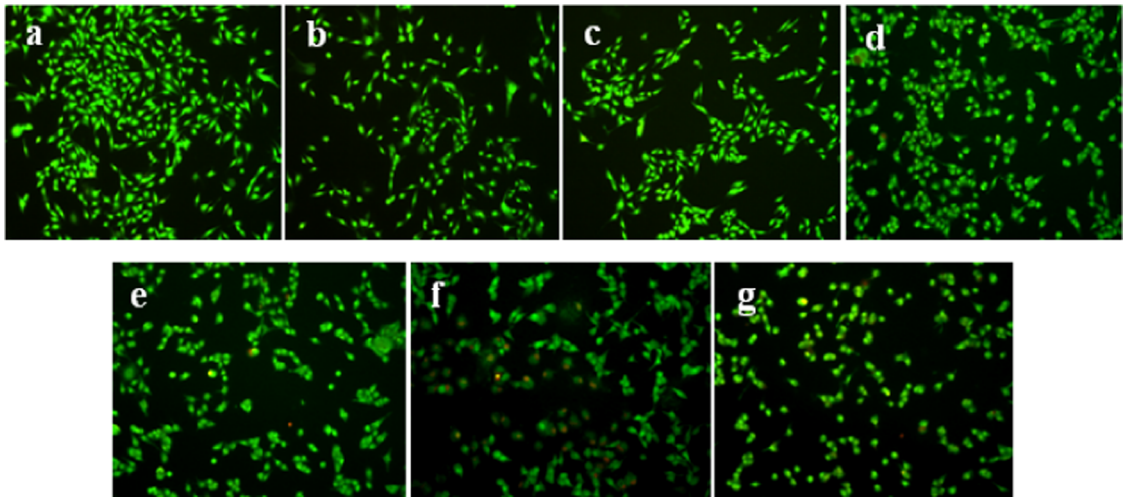

Figure 10. AO/EB staining of mouse fibroblast cells 3T3 of each administration group: (a) no treatment control group, (b) Span-PEG microbubble group, (c) Span-PEG-composited CNTs microbubble, (d) Span-PEG-composited Fe_3O_4−CNT microbubble, (e) Span-PEG-composited CNTs−DOX microbubble, (f) Span-composited Fe_3O_4−CNTs−DOX microbubble, and (g) the free DOX group.

fibroblast 3T3 cells for 24 h; free drug DOX, Span-PEG-composited Fe_3O_4−CNTs−DOX microbubbles, and Span-PEG-composited CNTs−DOX microbubbles had cytotoxic effects on SMMC-7721 cells and 3T3 cells, which had a significant difference in comparison with the Span-PEG microbubble group ($P < 0.05$). Moreover, the inhibition effect of free drug DOX on SMMC-7721 cells and 3T3 cells was most obvious, indicating that DOX was obviously toxic to normal cells while it inhibited tumor cells. Span-PEG-composited Fe_3O_4 CNTs−DOX microbubbles and Span-PEG-composited CNTs−DOX microbubbles had significantly lower inhibitory effects on normal mouse fibroblast 3T3 cells than on liver cancer SMMC-7721 cells, indicating that drug loading on CNTs and coating in the Span-PEG membrane material could reduce the direct stimulation effect of drugs on normal cells and decrease toxicity.

Different experiment groups respectively induced the apoptosis of SMMC-7721 cells, and the changes in cell morphology are shown in Figure 9. Acridine orange (AO) can penetrate the whole cell membrane and dye the nucleus of living cells, resulting in uniform green fluorescence. The nuclei of apoptotic cells were stained with yellow-green and bright green fluorescence by AO due to chromatin condensation or fragmentation. Ethidium bromide (EB) can only stain cells with incomplete membranes and cause the cells to emit orange-red fluorescence. Four cell morphologies were observed under fluorescence microscopy: living cells (VN), green nuclear chromatin with a normal structure; early apoptotic cells (VN), green nuclear chromatin with pyknosis or round bead shape; nonapoptotic dead cells (NVN), orange-red nuclear chromatin with a normal structure; and late apoptotic cells (NVN), orange-red nuclear chromatin with pyknosis or round bead shape. Figure 9a−d shows more number of adherent cells, no change in cell morphology, a clear cell outline, a close connection between cells, nuclear chromatin with green fluorescence and normal structure, the vast majority of living cells (VN) in the control group, Span-PEG microbubbles, Span-PEG-composited CNT microbubbles,

https://dx.doi.org/10.1021/acsomega.0c03325
ACS Omega 2020, 5, 31525−31534

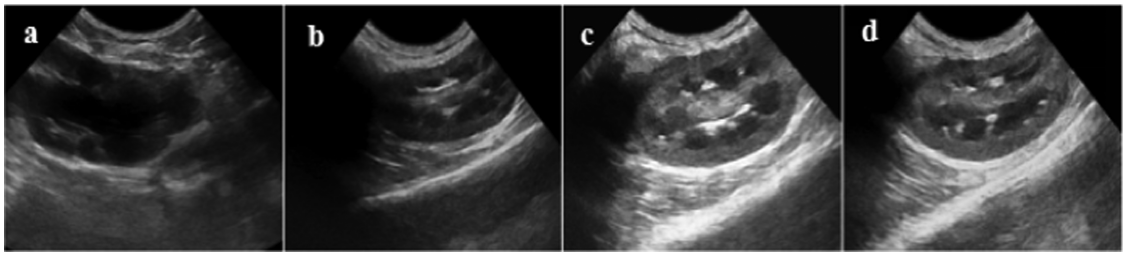

Figure 11. Ultrasonic imaging effect of rabbit kidney after injection of different contrast agents: (a) saline, (b) Span-PEG microbubble, (c) Span-PEG-composited CNT microbubble, and (d) Span-PEG-composited Fe_3O_4−CNTs−DOX microbubble.

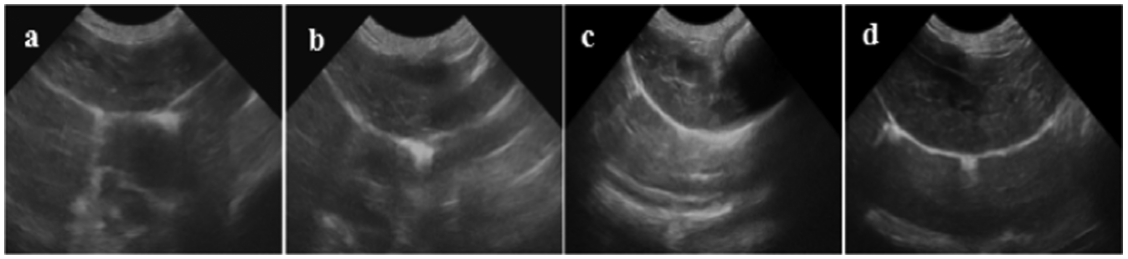

Figure 12. Ultrasonic imaging effect of rabbit liver after injection of different contrast agents: (a) saline, (b) Span-PEG microbubble, (c) Span-PEG-composited CNT microbubble, and (d) Span-PEG-composited Fe_3O_4−CNTs−DOX microbubble.

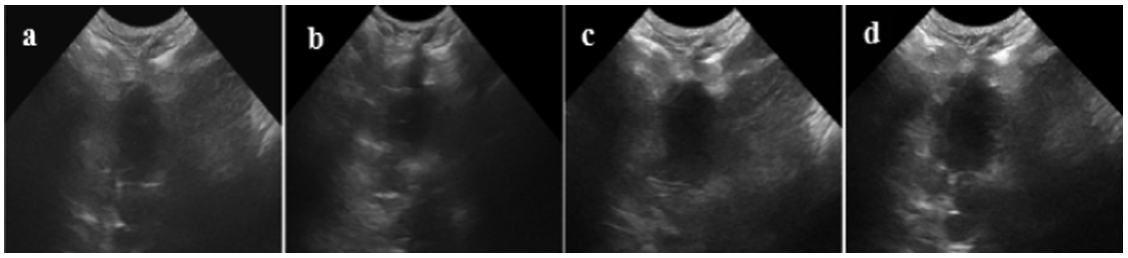

Figure 13. Ultrasonic imaging effect of rabbit heart after injection of different contrast agents: (a) saline, (b) Span-PEG microbubble, (c) Span-PEG-composited CNT microbubble, and (d) Span-PEG-composited Fe_3O_4−CNTs−DOX microbubble.

and Span-PEG-composited Fe_3O_4−CNTs microbubbles, which indicated that the Span-PEG membrane material and the Fe_3O_4−CNTs targeted drug system could not affect the growth of tumor cells. Figure 9e,f shows the cell shrinkage, a large number of early apoptotic cells with nuclear chromatin of green fluorescence and pyknotic or round bead shape, the appearance of apoptotic bodies, and a part of nonapoptotic dead cells with orange-red and normal-structured nuclear chromatin (NVN) for Span-PEG-composited CNTs−DOX microbubbles and Span-PEG-composited Fe_3O_4−CNTs−DOX microbubbles. After the free DOX treatment (Figure 9g), the cell boundaries were blurred, a large number of late apoptotic cells (NVA) with damaged cell membranes were stained with EB, and the nuclear chromatin was orange-red with a pyknotic or spherical shape. It can be seen that both Span-PEG-composited CNTs−DOX microbubbles and Span-PEG-composited Fe_3O_4−CNTs−DOX microbubbles could inhibit the proliferation of SMMC-7721 cells by inducing the apoptosis of tumor cells, and there was no significant difference in comparison with the drug DOX. This indicated that the prepared Span-PEG-composited Fe_3O_4−CNTs−DOX microbubbles had good drug activity and could effectively inhibit the proliferation of tumor cells.

Different experiment groups respectively induced apoptosis of mouse fibroblast 3T3 cells, and the morphological changes of cells are shown in Figure 10. No treatment control group, Span-PEG microbubbles, Span-PEG-composited CNT microbubbles, and Span-PEG-composited Fe_3O_4−CNTs microbubbles in Figure 10a−d indicated more number of cells, cell morphology with a spindle, intact cell membrane, clear cell boundary, adherent and radiating cells, and nuclear chromatin with green fluorescence and normal structure, which indicated the active cell DNA synthesis. It can be seen that the carrier used in the experiment has no obvious cytotoxic effect on mouse fibroblast 3T3 cells. Span-PEG-composited Fe_3O_4−CNTs−DOX microbubbles in Figure 10f indicated the decrease of cell number, the poor cell state, a slightly irregular cell morphology, early apoptotic cells with nuclear chromatin of green fluorescence and pyknosis or round bead shape, and a part of nonapoptotic dead cells (NVN) with a normal structure. Span-PEG-composited CNTs−DOX microbubbles (Figure 10e) indicated a large number of nonapoptotic dead cells (NVN) with orange-red and normal-structured nuclear chromatin and the increased early apoptotic cells. After the free DOX treatment (Figure 10g), the cell boundaries were blurred, a large number of late apoptotic cells (NVA) with damaged cell membranes were stained with EB, and the nuclear chromatin was orange-red with pyknosis or spherical shape. It can be seen that Span-PEG-composited Fe_3O_4−CNTs−DOX microbubbles and Span-PEG-composited CNTs−DOX microbubbles could affect the cycle of mouse fibroblast 3T3 cells and induce cell apoptosis, while its induction of apoptosis

https://dx.doi.org/10.1021/acsomega.0c03325
ACS Omega 2020, 5, 31525−31534

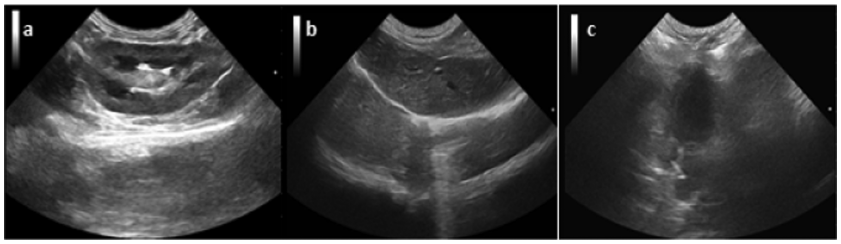

Figure 14. Ultrasound imaging of rabbit kidney (a), liver (b), and heart (c) after the injection of Span-PEG composite Fe_3O_4−CNTs−DOX microbubble under the magnetic field.

effect was lower than that of free DOX, indicating that the composite microbubbles could reduce the toxic effect of DOX on normal cells in agreement with Figure 8.

Figures 11 and 12−13 respectively show ultrasound imaging images of the kidney, liver, and heart of rabbits. Figures 11a and 13a show the ultrasound imaging images after the injection of normal saline. It can be found from Figures 11a and 13a that the ultrasound signals in the kidneys, livers, and hearts of rabbits were weak and could not be developed effectively. Figures 11b and 13b show the ultrasound imaging images of rabbits after Span-PEG microbubbles injection. It can be seen from Figures 11b and 13b that the ultrasound signals in the kidney, liver, and heart of rabbits were enhanced and could be developed effectively. Figures 11c and 13c show the ultrasound imaging images of rabbits after the injection of Span-PEG-composited CNTs microbubbles. After a few seconds of injection, the blood vessels in the kidney, liver, and heart of rabbits rapidly filled, dense echo signals were detected, and the contrast of ultrasound development was significantly increased, indicating that CNTs could enhance the ultrasound development of Span-PEG microbubbles. Figures 11d and 13d show the ultrasound imaging images of rabbits after the injection of Span-PEG-composited Fe_3O_4−CNTs−DOX microbubbles. After a few seconds of injection, the blood vessels in the kidney, liver, and heart of rabbits were rapidly filled, the ultrasound development effect was enhanced with a clear profile of each organ, and the signal intensity was similar to that of Span-PEG-composited CNTs microbubbles. At the same time, some acute toxicity symptoms such as palpitations, arrhythmia, pulmonary embolism, asthma, or even death were not observed in rabbits during the injection of microbubbles through the auricular vein, which fully verified the good biological safety of Span-PEG microbubbles, Span-PEG-composited CNT microbubbles, and Span-PEG-composited Fe_3O_4−CNTs−DOX microbubbles.

Compared with the physiological saline group (Figures 11a and 13a), the kidney, liver, and heart of rabbit all showed a good ultrasonic signal response after the injection of Span-PEG microbubbles (Figures 11b and 13b), Span-PEG-composited CNT microbubbles (Figures 11c and 13c), and Span-PEG-composited Fe_3O_4−CNTs−DOX microbubbles (Figures 11d and 13d). The ultrasonic signal intensity of Span-PEG-composited CNT microbubbles was similar to that of Span-PEG-composited Fe_3O_4−CNTs−DOX microbubbles, and their development effect and image brightness were significantly higher than those of the saline control group and Span-PEG microbubbles, indicating that the addition of CNTs in the Span-PEG microbubbles was beneficial to enhance the contrast effect, while the ultrasonic development effect of CNTs modified by Fe_3O_4 did not change.

After the injection of Span-PEG-composited Fe_3O_4−CNTs−DOX microbubbles under an additional magnetic field, ultrasonic imaging effects of kidney, liver, and heart in rabbit are shown in Figure 14a−c. On comparing Figures 11d and 13d, it was observed that the magnetic field could make the concentration of composite microbubbles higher in a particular part, raise the ultrasonic imaging contrast and definition, and extend the effective ultrasonic imaging time, which were more conducive to observe and diagnose. It was shown that CNTs modified by Fe_3O_4 could realize the effect of targeted ultrasound imaging. At the same time, the rabbits did not show acute toxic symptoms such as palpitations, arrhythmia, pulmonary embolism, asthma, or even death during the contrast-enhanced ultrasound, which fully verified the good biosafety of Span-PEG-composited Fe_3O_4−CNTs−DOX microbubbles.

3. CONCLUSIONS

The obtained Span-PEG-composited Fe_3O_4−CNTs−DOX microbubbles significantly enhanced the ultrasound imaging of the kidney, liver, and heart of rabbits. The composite microbubbles can be enriched in the blood vessels under the effect of an external magnetic field; as a result, the ultrasonic imaging signal can be enhanced and the ultrasonic development time can be prolonged. Span-PEG-composited Fe_3O_4−CNTs−DOX microbubbles inhibited the proliferation of liver cancer SMMC-7721 cells and normal mouse fibroblast 3T3 cells. Compared with free DOX, Span-PEG-composited Fe_3O_4−CNTs−DOX microbubbles reduced the direct toxic effect of DOX on normal cells. Span-PEG-composited Fe_3O_4−CNTs−DOX microbubbles significantly affected the apoptosis cycle of liver cancer SMMC-7721 cells and had a certain adjuvant therapeutic effect. Span-PEG-composited Fe_3O_4−CNTs microbubbles were safe and stable at the maximum dose, and the maximum tolerance of mice was 450 times higher. The obvious systemic allergic reaction did not appear when mice were injected with Span-PEG-composited Fe_3O_4−CNTs−DOX microbubbles for 21 days. After intramuscular injection of Span-PEG-composited Fe_3O_4−CNTs−DOX microbubbles into the back of mice, obvious muscle stimulation was not observed, meeting the clinical requirements for a medical ultrasound contrast agent.

4. EXPERIMENTAL SECTION

4.1. Preparation of Span-PEG-Composited Fe_3O_4−CNTs−DOX Microbubbles. First, an Fe_3O_4−CNTs magnetic targeting complex was prepared by an in situ liquid phase synthesis method. Typically, 0.45 g of CNTs was dispersed in distilled water under ultrasound and transferred to a three-necked flask. Typically, 0.47 g of $FeCl_3$, 0.23 g of $FeCl_2$, and an appropriate amount of PEG1500 were also added to a three-

https://dx.doi.org/10.1021/acsomega.0c03325
ACS Omega 2020, 5, 31525−31534

necked flask and mixed with CNTs. Meanwhile, 4 mg·mL^{-1} NaOH solution was slowly dropped into the above system placed in a 60 °C water bath until the reaction solution was alkaline, stirring for 20 min and aging at 80 °C for 30 min. After the end of the reaction, the magnet was attached to the bottom of the three-necked flask to gather magnetic CNTs, the supernatant was discarded, and the CNTs−Fe_3O_4 magnetic targeting complex was obtained by washing with distilled water and freeze-drying.

Second, 20 mg of the CNTs−Fe_3O_4 complex was dispersed in an appropriate amount of distilled water under ultrasound. Typically, 35 mg of DOX was dissolved in an appropriate amount of anhydrous ethanol and added into the dispersion solution of the CNTs−Fe_3O_4 complex. The mixture system was stirred at 30 °C for 180 min, filtered, washed, and freeze-dried, and the Fe_3O_4−CNTs−DOX complex was obtained.

Finally, 30 mg of the Fe_3O_4−CNTs−DOX complex was evenly dispersed in 10 mL of phosphate-buffered saline (PBS) solution. Typically, 450 mg of Span60, 450 mg of PEG1500, and 900 mg of NaCl were ground, well mixed in a mortar, and then transferred to a beaker; 40 mL of PBS was added. This system was heated to 80 °C and stirred for 30 min, and the dispersion solution of the Fe_3O_4−CNTs−DOX complex was added. The obtained mixing system was stirred for 15 min and treated for 6 min under a power of 600 W with an ultrasonic cell crushing instrument (FS1500T, Shanghai Shengxi Ultrasonic Instrument Co., Ltd.), and nitrogen was introduced at the same time. After acoustic vibration treatment, the above mixing system was added to the funnel and washed with an equal amount of PBS three times. The medium microbubble suspension was collected and freeze-dried, and Span-PEG-composited Fe_3O_4−CNTs−DOX microbubbles were obtained.

4.2. Acute Toxicity Test. Freeze-dried powders of Span-PEG-composited Fe_3O_4−CNTs microbubbles were processed into a suspension with the degassing physiological saline. Specific pathogen-free Kunming (SPF KM) mice were selected, half male and half female, and randomly divided into low-, medium-, and high-dose groups: 2000, 4000, and 8000 mg·kg^{-1}. Three mice in each group were intraperitoneally injected with Span-PEG-composited Fe_3O_4−CNTs microbubbles once (0.1 mL·10 g^{-1}) at the same dose, and the observation was maintained for 72 h, and the number of dead animals was recorded. The experiment was repeated at a certain dose ratio between the two groups until the groups of 3/3 death and 0/3 death were found, and the maximum dose without mouse death (Dn) and the minimum dose that causes all mice to die (Dm) were obtained.

The Dn value was selected as the maximum dose of mice for the safety limit test based on the objective necessity and humanitarian principle. Twenty KM mice, half male and half female, were randomly selected and injected once at a maximum dosage of the same volume. The toxicity, behavioral, and weight changes were recorded after observation of 14 days. The maximum tolerance of multiple formula was used for conversion.

4.3. Allergic Test. Ten KM mice, half male and half female, were injected with 10 mg·mL^{-1} (0.2 mL) Span-PEG-composited Fe_3O_4−CNTs microbubble suspension liquid every 2 days three times. Then, they were randomly divided into two groups: group 1: intraperitoneal injection after 14 days of the first injection; group 2: intraperitoneal injection after 21 days of the first injection. Scratching, sneezing, bristling, convulsion, dyspnea, urinary and fecal incontinence, shock, and death at 2 h after injection were observed.

4.4. Biocompatibility Experiment. KM mice (SPF grade, Changchun Yisi Experimental Animal Technology Co. Ltd.) were randomly divided into two groups. Mice of the dose group were injected with 0.2 mL of Span-PEG-composited Fe_3O_4−CNTs microbubbles (100 mg·mL^{-1}), and mice of the control group were injected with 0.2 mL of normal saline.

At 2, 4, 10, 22, and 30 days after intramuscular injection, the mice from the above two groups were sacrificed by removing cervical vertebrae, and the stimulus response of local tissues at the injection site was visually observed. The muscle tissue that contacted with Span-PEG-composited Fe_3O_4−CNTs microbubbles at the injection site was taken out and fixed in a formalin solution. Paraffin sections were prepared and placed under an optical microscope (×200), and the tissue changes at the injection site were observed and recorded for each group.

4.5. Cell Culture. Hepatoma cell line SMMC-7721 was used for the in vitro antitumor test, and mouse fibroblast cell 3T3 was used as a comparison group. The 1640 Roswell Park Memorial Institute (RPMI) complete medium containing 10% fetal bovine serum, 1% double antibodies (penicillin and streptomycin), and 1% L-glutamine was used. The two kinds of cells were normally cultured at 37 °C, 5% CO_2 (V%), and under completely saturated humidity.

4.6. Antitumor Cell Activity of the Composite Microbubbles by the CCK-8 Method. SMMC-7721 cells were inoculated into 96-well plates at 1 × 10^4 per hole until cells completely adhered to the wall. Freeze-dried powders of Span-PEG-composited Fe_3O_4−CNTs−DOX microbubbles were prepared into suspension liquid of 2.5, 5, 7.5, 10, 15, 20, 30, and 40 mg·mL^{-1}. Each hole was added with 100 μL of the microbubble suspension liquid, and three parallel samples were set for each microbubble concentration. At 12, 24, and 48 h after incubation, the culture system was sucked out and washed with PBS. Briefly, 10 μL of the CCK-8 solution and 90 μL of RPMI1640 medium were added to each well, and the color reaction was developed for 1 h. The absorbance of each hole was detected using an enzyme micrometer.

96-well plates were set as follows: DOX group, Span-PEG microbubble group, Span-PEG-composited Fe_3O_4−CNTs−DOX microbubble group, Span-PEG-composited CNTs−DOX microbubble group, Span-PEG-composited Fe_3O_4−CNTs microbubble group, Span-PEG-composited CNT microbubble group, and control group without drugs; then, six parallel samples in each group were set up. The proliferation inhibition rate of seven groups of samples on SMMC-7721 cells was drawn by the CCK-8 method.

Using the same method, the optimal-state 3T3 cells under the logarithmic growth period were taken as a comparison. The toxicity of the different microbubbles on normal mouse fibroblast 3T3 cells was detected according to the same group as mentioned above.

4.7. Effects of Different Composite Microbubbles on Different Cell Apoptosis by AO/EB Fluorescence Staining. SMMC-7721 cells were inoculated into 96-well plates at 1 × 10^4 per hole until cells completely adhered to the wall. The free DOX group, Span-PEG microbubble group, Span-PEG-composited Fe_3O_4−CNTs−DOX microbubbles, Span-PEG-composited CNTs−DOX microbubbles, Span-PEG-composited Fe_3O_4−CNTs microbubbles, Span-PEG-composited CNT microbubbles group, and the control group without drugs were set. After incubating each group, they were

https://dx.doi.org/10.1021/acsomega.0c03325
ACS Omega 2020, 5, 31525−31534

washed twice with PBS and the AO/EB staining agent was added to each well at 120 μL per well. The results were observed under an inverted fluorescence microscope. The experiment was repeated independently three times in each group.

By the same method, mouse fibroblast 3T3 cells under the logarithmic growth period were taken as a comparison, and each group of microbubbles was added. After AO/EB staining, the results were observed under an inverted fluorescence microscope.

4.8. Ultrasonic Imaging Experiment of Span-PEG-Composited Fe_3O_4−CNTs−DOX Microbubbles. Experimental groups were set as follows: normal saline control group, Span-PEG microbubble group, Span-PEG-composited CNTs microbubble group, and Span-PEG-composited Fe_3O_4−CNTs−DOX microbubbles. Each group of microbubble freeze-dried powders was prepared with degassed physiological saline to the suspension with a concentration of 60 mg·mL^{-1}. A peripheral venous channel was established in the periauricular vein of the rabbit. Different groups of microbubbles and normal saline of 1 mL were injected, respectively. The echo intensity enhancement of the heart, liver, and kidney of rabbit was dynamically observed and recorded with the Doppler color ultrasound imaging system (color Doppler ultrasound imaging system, S40, China)

AUTHOR INFORMATION

Corresponding Author

Jinjing Li − *Pharmacy College, Jiamusi university, Jiamusi 154007, China*; Phone: 13846184696; Email: jmsuljj@qq.com

Authors

Jie Zhang − *Pharmacy College, Jiamusi university, Jiamusi 154007, China*; orcid.org/0000-0002-4257-696X

Zhongtao Liu − *Pharmacy College, Jiamusi university, Jiamusi 154007, China*

Shujing Zhou − *Pharmacy College, Jiamusi university, Jiamusi 154007, China*

Yang Teng − *Pharmacy College, Jiamusi university, Jiamusi 154007, China*

Xiangyu Zhang − *Pharmacy College, Jiamusi university, Jiamusi 154007, China*

Complete contact information is available at: https://pubs.acs.org/10.1021/acsomega.0c03325

Notes

The authors declare no competing financial interest.

ACKNOWLEDGMENTS

This work was supported by an excellent innovation team based on the basic scientific research vocational cost for the provincial undergraduate universities in Heilongjiang (No. 2018-KYYWF-0914), scientific research initiation fund of postdoctoral researchers settled down in Heilongjiang (31303120), Heilongjiang health department project (2019-291), basic research project of Heilongjiang basic scientific research operating expenses (2018-KYYWF-0946), and Jiamusi University doctoral program (JMSUZB2018-02).

REFERENCES

(1) Guo, L.; Shi, D.; Meng, D.; Shang, M.; Sun, X.; Zhou, X. Y.; Liu, X.; Zhao, Y. D.; Li, J. New FH peptide-modified ultrasonic nanobubbles for del-ivery of doxorubicin to cancer-associated fibroblasts. *Nanomedicine* **2019**, 2957−2971.

(2) Yeo, Y. Battling with environments: during delivery to targeted tissues with particles and functional biomaterials. *Ther. Delivery* **2010**, *1*, 757−761.

(3) Wang, Y.; Bi, K.; Shu, J. X.; Liu, X. J.; Xu, J. F.; Deng, G. Y. Ultrasound-controlled DOX-SiO_2 nanocomposites enhance the antitumour efficacy and attenuate the toxicity of doxorubicin. *Nanoscale* **2019**, *11*, 4210−4218.

(4) Wang, L.; Shi, J.; Jia, X.; Liu, R. Y.; Wang, H.; Wang, Z.; Li, L.; Zhang, J.; Zhang, C. F.; Zhang, Z. NIR/pH□responsive drug delivery of functionalized single-walled carbon nanotubes for potential application in cancer chemo-photothermal therapy. *Pharm. Res.* **2013**, *30*, 2757−2771.

(5) Prakash, S.; Malhotra, M.; Shao, W.; Tomaro-Duchesneau, C.; Abbasi, S. Polymeric nanohybrids and functionalized carbon nanotubes as drug delivery carriers for cancer therapy. *Adv. Drug Delivery Rev.* **2011**, *63*, 1340−1351.

(6) Pruthi, J.; Mehra, N. K.; Jain, N. K. Macrophages targeting of amphotericin B through mannosylated multiwalled carbon nanotubes. *J. Drug Targeting* **2012**, *20*, 593−604.

(7) Chaschin, I. S.; Grigorev, T. E.; Gallyamov, M. O.; Khokhlov, A. R. Directd eposition of chitosan macromolecules on a substrate from solutions in supercritical carbon dioxide: Solubility and conformational analysis. *Eur. Polym. J.* **2012**, *48*, 906−918.

(8) Yan, Y.; Wang, R. Z.; Hu, Y.; Sun, R. Y.; Song, T.; Shi, X. Y.; et al. Stacking of doxorubicin on folic acid-targeted multiwalled carbon nanotubes for in*vivo* chemotherapy of tumors. *Drug Delivery* **2018**, *25*, 1607−1616.

(9) Singh, R. P.; Sharma, G.; Sonali; Singh, S.; Patne, S. C. U.; Pandey, B. L.; Koch, B.; Muthu, M. S. Effects of transferrin conjugated multi-walled carbon nanotubes in lung cancer delivery. *Mater. Sci. Eng., C* **2016**, *67*, 313−325.

(10) Liu, Z.; Yang, K.; Lee, S. T. Single-walled carbon nanotubes in biomedical imaging. *J. Mater. Chem.* **2011**, *21*, 586−598.

(11) Zhao, X. B.; Tian, K.; Zhou, T.; Jia, X.; Li, J. G.; Liu, P. PEGylated multi-walled carbon nanotubes as versatile vector for tumor-specific intracellular triggered release with enhanced anticancer efficiency: Optimization of length and PEGylation degree. *Colloids Surf., B* **2018**, *168*, 43−49.

(12) Yu, B. D.; Tan, L.; Zheng, R. H.; Tan, H.; Zheng, L. X. Targeted delivery and controlled release of Paclitaxel for the treatment of lung cancer using single-walled carbon nanotubes. *Mater. Sci. Eng., C* **2016**, *68*, 579−584.

(13) Rathod, V.; Tripathi, R.; Joshi, P.; Jha, P. K.; Bahadur, P.; Tiwari, S. Paclitaxel Encapsulation into Dual-Functionalized Multi-Walled Carbon Nanotubes. *AAPS PharmSciTech* **2019**, *20*, 51−64.

(14) Delogu, L. G.; Vidili, G.; Venturelli, E.; Venturelli, E.; Menard-Moyon, C.; Zoroddu, M. A.; Pilo, G.; Nicolussi, P.; Ligios, C.; Bedognetti, D.; et al. Functionalized multiwalled carbon nanotubes as ultrasound contrast agents. *Proc. Natl. Acad. Sci. U.S.A.* **2012**, *109*, 16612−16617.

(15) Gu, F.; Hu, C. L.; Xia, Q. M.; Gong, C. A.; Gao, S.; Chen, Z. J. Aptamer-conjugated multi-walled carbon nanotubes as a new targeted ultrasound contrast agent for the diagnosis of prostate cancer. *J. Nanopart. Res.* **2018**, *20*, No. 303.

(16) Lv, Y.; Ding, G. B.; Zhai, J. H.; Guo, Y.; Nie, G. J.; Xu, L. A superparamagnetic Fe_3O_4-loaded polymeric nanocarrier for targeted delivery of evodiamine with enhanced antitumor efficacy. *Colloids Surf., B* **2013**, *110*, 411−418.

(17) Wang, Q. H.; Jiao, L. F.; Du, H. M.; Wang, Y. J.; Yuan, H. T. Fe_3O_4 nanoparticles grown on graphene as advanced electrode materials for supercapacitors. *J. Power Sources* **2014**, *245*, 101−106.

(18) Peng, X.; Luan, Z.; Di, Z.; Zhang, Z.; Zhi, C. Carbon nanotubes-iron oxides magnetic composites as adsorbent for removal of Pb(II) and Cu(II) from water. *Carbon* **2005**, *43*, 880−883.

(19) Zhang, J.; Song, L. M.; Zhou, S. J.; Hu, M.; Jiao, Y. F.; Teng, Y.; Wang, Y.; Zhang, X. Y. Enhanced ultrasound imaging and anti-tumor in vivo properties of Span-Polyethylene glycol with folic acid-carbon

https://dx.doi.org/10.1021/acsomega.0c03325
ACS Omega 2020, 5, 31525−31534

nanotubes-paclitaxel multifunctional microbubbles. *RSC Adv.* **2019**, *9*, 35345−35355.
(20) Zhang, J.; Yang, J. Z.; Zhang, H. M.; Zhou, S. J.; Li, J.; Zhang, X. Y. A new Span-PEG-composited Fe_3O_4-CNT as a multifunctional ultrasonic contrast agent based on inflammatory and thrombotic niduses. *RSC Adv.*, 2020, online delivering.

https://dx.doi.org/10.1021/acsomega.0c03325
ACS Omega 2020, 5, 31525−31534